Published in final edited form as:
FASEB J. 2024 January ; 38(1): e23355. doi:10.1096/fj.202301948R.

Biochemical characterization of the *Drosophila* insulin receptor kinase and longevity-associated mutants

Harini Krishnan[1], **Sultan Ahmed**[1], **Stevan R. Hubbard**[2], **W. Todd Miller**[1,3]

[1]Department of Physiology and Biophysics, School of Medicine, Stony Brook University, Stony Brook, New York, USA

[2]Department of Biochemistry and Molecular Pharmacology, New York University Grossman School of Medicine, New York, New York, USA

[3]Department of Veterans Affairs Medical Center, Northport, New York, USA

Abstract

Drosophila melanogaster (fruit fly) insulin receptor (D-IR) is highly homologous to the human counterpart. Like the human pathway, D-IR responds to numerous insulin-like peptides to activate cellular signals that regulate growth, development, and lipid metabolism in fruit flies. Allelic mutations in the D-IR kinase domain elevate life expectancy in fruit flies. We developed a robust heterologous expression system to express and purify wild-type and longevity-associated mutant D-IR kinase domains to investigate enzyme kinetics and substrate specificities. D-IR exhibits remarkable similarities to the human insulin receptor kinase domain but diverges in substrate preferences. We show that longevity-associated mutations reduce D-IR catalytic activity. Deletion of the unique kinase insert domain portion or mutations proximal to activating tyrosines do not influence kinase activity, suggesting their potential role in substrate recruitment and downstream signaling. Through biochemical investigations, this study enhances our comprehension of D-IR's role in *Drosophila* physiology, complementing genetic studies and expanding our knowledge on the catalytic functions of this conserved signaling pathway.

Keywords

Drosophila; insulin receptor; kinetics; loss of function mutation; Sf9 cells; tyrosine kinase

Correspondence: W. Todd Miller, Department of Physiology and Biophysics, School of Medicine, Stony Brook University, Stony Brook, New York 11794-8661, USA. todd.miller@stonybrook.edu.

AUTHOR CONTRIBUTIONS

Harini Krishnan designed and conducted experiments, analyzed and interpreted data, and drafted and revised the manuscript. Sultan Ahmed conducted experiments and analyzed data. Stevan R. Hubbard designed research and revised the manuscript. W. Todd Miller conceived and designed research, obtained funding, and revised the manuscript.

DISCLOSURES

H.K., S.A., and W.T.M. declare no conflicts of interest. S.R.H. is a co-founder and scientific advisory board member of Ajax Therapeutics, Inc.

SUPPORTING INFORMATION

Additional supporting information can be found online in the Supporting Information section at the end of this article.

1 | INTRODUCTION

Insulin/IGF-1 signaling (IIS) is a highly conserved and fundamental cellular pathway that spans across diverse species. From insects like *Drosophila melanogaster* to mammals, the insulin receptor-signaling pathway plays a pivotal role in regulating key physiological processes such as growth, metabolism, and longevity.[1–5] This pathway begins with the binding of insulin or insulin-like peptides to their cognate receptors, activating a cascade of molecular events that involves trans-autophosphorylation of the kinase domain tyrosines, recruitment of downstream adaptor proteins, and activation of various intracellular effectors. Despite evolutionary differences, the core components and mechanisms underlying this pathway exhibit remarkable similarity across species, showcasing its essential role in maintaining metabolic homeostasis and cellular responses to nutrient availability. The conservation of insulin receptor signaling underscores its significance as a target for understanding pathologies like diabetes and aging, and highlights the utility of model organisms like *Drosophila* in unraveling its intricate molecular details.

In contrast to humans, the *Drosophila* IIS encompasses a single receptor known as the *Drosophila* insulin receptor (DInR or D-IR, as referred to in this paper). Various *Drosophila* insulin-like peptides (DILPs) have been characterized, and upon nutrient stimulation, they interact with D-IR to govern growth and development.[6,7] These DILPs are specific to different tissues and share both structural and functional similarities with human insulin and IGF-1 hormones.[6,8] Similar to their human counterparts, fully functional D-IR comprises two α- and two β-chains, forming a heterotetramer that becomes activated through intramolecular trans-autophosphorylation of the kinase domains.[9,10] Upon activation by DILPs, D-IR interacts with the homolog of the insulin receptor substrate (IRS), termed CHICO, which then engages in the activation of the *Drosophila* equivalent of phosphatidylinositol 3′-kinase, Dp110/p60, thereby modulating growth and longevity.[11]

However, distinct from the human receptor, D-IR possesses an additional C-terminal extension of 368 amino acids. This unique extension contains three tandem repeats of the YxxM motif. The YxxM motifs are generally found in the human insulin receptor substrate (IRS) proteins. IRS adaptor proteins are the primary cellular substrates for the human insulin and insulin-like growth factor 1 receptors (H-IR and IGF-1R, respectively). When phosphorylated, they bind phosphatidylinositol 3′-kinase (PI3K), Grb2, and other Src homology 2 (SH2) domain-containing proteins. Although CHICO also has YxxM motifs, the D-IR's own YxxM motifs are able to independently recruit and activate PI3K to regulate cell survival.[12] The C-terminal extension undergoes cell-specific proteolytic cleavage, leading to the generation of a shorter isoform with possibly different signaling capabilities than the extended form.[9]

D-IR kinase domain (D-IRK) is strikingly similar to the human insulin receptor kinase domain (H-IRK), with about 60% amino acid identity (Figure 1A). Amino acids in the ATP-binding site, catalytic loop, and activation loop are identical in D-IRK and H-IRK. Three tyrosine autophosphorylation sites in the activation loop that are critical for regulation of H-IRK (and IGF-1RK) are conserved in D-IRK.[14–16] Superposition of the AlphaFold-predicted structure of the active form of D-IRK and the crystallized active conformation of

H-IRK shows a significant overlap in the structural elements that govern the activity of these two kinases (Figure 1B).[15,17] A divergent feature of the D-IRK is the conspicuous presence of a longer kinase insert region (Figure 1A).[9] This region contains two tyrosine residues, one of which bears the YxN motif, which typically acts as a recognition site for the SH2 domain of Grb2. H-IRK has a smaller kinase insert domain and lacks these tyrosines.

Homozygous null and loss-of-function alleles in D-IR lead to significant growth and developmental defects, as well as lethality in *Drosophila*.[6,9–11,18] However, partial loss of function mutations and weak heterozygous combinations extend life expectancy and lipid content with or without reduction in body size in adult fruit flies.[6,10,19] The InR^{353} allele, which bears a mutation in the kinase insert region, is particularly interesting. Eye-specific mutation in this allele causes a reduction in eye tissue and head size[6] but dramatically extends the lifespan and fecundity of adult fruit flies when heterozygous with wild-type.[10] Smaller increases in life expectancy are observed for heterozygotes with the InR^{211} allele, in which the mutation occurs in the C-lobe, or with the InR^{74} allele, in which the mutation is in the activation loop of D-I RK. Taken together, these genetic studies in *Drosophila* show that partial loss of function of D-IR has the potential to suppress severe growth and developmental defects but extend lifespan in *Drosophila*. These effects could potentially be brought about by defects in the intrinsic catalytic activity of D-IRK, or alternatively by ineffective substrate recruitment and consequent downstream signaling.

For this study, we expressed and purified wild-type D-IRK to characterize its catalytic activity and substrate specificity. We also utilized this strategy to examine the impact on kinase activity of substitution mutations that are involved in *Drosophila* growth and lifespan. We show that two mutations that are known to decrease head size but elevate lifespan in *Drosophila* indeed inhibit kinase activity and thermal stability. Interestingly, deletion of the unique additional portion of the *Drosophila* kinase insert domain or a mutation proximal to the activating tyrosines did not affect kinase activity, suggesting a possible role in substrate recruitment and downstream signaling. Our biochemical investigations can complement genetic studies to dissect the role of D-IR in *Drosophila* physiology.

2 | MATERIALS AND METHODS

2.1 | D-IRK constructs

A cDNA encoding the tyrosine kinase domain (amino acids 1358 to 1672) of *Drosophila* insulin-like receptor (NCBI Reference Sequence: NP_524436.2) was synthesized commercially (GenScript Corp.) and cloned into the BamHI and NotI sites of pFastbac-HTb (ThermoFisher). Mutations R1467C, I1544F, G1599R, and ΔKI were made in the wild-type (WT) D-IRK construct with the appropriate primers (IDT, listed in Table S1) using the QuikChange II XL site-directed mutagenesis kit (Agilent 200522) according to manufacturer's protocol. WT or mutant pFastbac vectors were used to generate recombinant baculovirus for protein expression and purification.

2.2 | Expression and purification of D-IRK

Recombinant baculoviruses encoding WT or mutant forms of the N-terminally His-tagged D-IRK were generated according to the Bac-to-Bac expression protocol (ThermoFisher) and were used to infect 600 mL of *Spodoptera frugiperda* (*Sf*9, RRID:CVCL_0549) cells at 1.8 × 10^6 cells/mL. The infected cells were harvested after 3 days and pellets were stored at −80°C. For protein purification using immobilized metal affinity chromatography, frozen pellets were thawed in lysis buffer containing 50 mM Tris–HCl, pH 8.5, 100 mM NaCl, 1% NP-40 substitute or IGEPAL CA-630, 5 mM β-mercaptoethanol, 10 μg/mL leupeptin, 10 μg/mL aprotinin, and 1 mM PMSF, and then disrupted in a French pressure cell at 18000 psi. The cell lysates were clarified by centrifugation at 40 000*g* for 30 min, filtered with 5 μm and 0.45 μm filters, and then applied to 4.5 mL of Ni-NTA resin (Qiagen 30230) in a column. The resin was washed with 50 mL buffer A (20 mM Tris–HCl buffer, pH 8.5, 0.5 M NaCl, 10 mM imidazole, 10% glycerol, and 5 mM β-mercaptoethanol), 50 mL buffer B (20 mM Tris–HCl buffer, pH 8.5, 10% glycerol, and 5 mM β-mercaptoethanol), and again with 100 mL buffer A. His-tagged D-IRK was then serially eluted in 25 to 100 mM imidazole in buffer with 20 mM Tris–HCl pH 8.5, 10% glycerol, and 5 mM β-mercaptoethanol. The fractions containing D-IRK were pooled, buffer exchanged in 20 mM Tris–HCl, pH 8.5, and 10% glycerol to remove imidazole, and concentrated using a 10-kD-molecular-weight cutoff membrane (Millipore PLGC06210) fitted in an Amicon® stirred cell. Concentrated samples in protein storage buffer containing 20 mM Tris–HCl, pH 8.5, and 40% glycerol were flash frozen in liquid N_2 and stored in −80°C or further purified and analyzed using a HiLoad Superdex 75 16/600 pg column (Cytiva 28989333) in an ÄKTA pure 25 chromatography system. Purified protein samples were verified for molecular weight and purity using SDS-PAGE followed by Coomassie staining and concentrations were determined using the Bradford method (Biorad 5000205). Expression and purification of H-IRK have been previously described.[20]

2.3 | In vitro kinase assays

Kinase activities of D-IRK and mutants were measured using phosphocellulose paper-binding assays with [γ−^{32}P]-ATP. Twenty-five microliter reactions were carried out in kinase assay buffer containing a final concentration of 25 mM HEPES (pH 7.5), 4.67 mM $MgCl_2$, 6.35 mM $MnCl_2$, 0.5 mM DTT, 0.05 mM Na_3VO_4, 1 nM BSA, 0.2 mM ATP, 0.5 mM peptide substrate, and 20–50 cpm/pmol of [γ−^{32}P]-ATP or as indicated in the figure legends. Reactions were initiated with the addition of buffer cocktail to enzyme and incubated for 10 min at 30°C unless otherwise mentioned. The reactions were quenched by the addition of 45 μL 10% trichloroacetic acid, vortexed, and centrifuged for 2 min. After centrifugation, 30–35 μL of the supernatants were spotted on Whatman phosphocellulose P81 paper and washed three times with ice-cold 0.5% phosphoric acid for 10 min each. After a final wash with acetone, the P81 papers were dried, and the incorporation of ^{32}P into the peptide was determined by scintillation counting. Synthetic peptide substrates for various kinases and IRS-1 used in these assays are in Tables 1 and 2. All crude peptide substrates were purified by reverse-phase high-pressure liquid chromatography, resuspended in buffer containing 50 mM Tris, pH 7.5, and concentrations measured using UV–Vis spectroscopy prior to use in kinase assays.

2.4 | Inhibitor screen and IC_{50} assays

Inhibitor screen and IC_{50} assays were carried out using the phosphocellulose paper-binding assay with [γ–^{32}P]-ATP as described above. Linsitinib (HY-10191) and Dasatinib (HY-10181) were obtained from MedChem Express, Lapatinib (094127) from Matrix Scientific, Erlotinib (S7786) and Vandetanib (S1046) from Selleckchem, and Staurosporine (S4400) from Sigma. Inhibitors were used at a final concentration of 10 μM (unless otherwise mentioned) for the inhibitor screen and a range of concentrations between 1 nM and 5 μM was used for linsitinib IC_{50} assays. Inhibitors were preincubated with the enzyme for not more than 10 min at room temperature before initiation of kinase reactions. DMSO was used as a negative control for these assays. IC_{50} values were calculated by non-linear regression analysis of the [inhibitor] versus response curves using GraphPad Prism 9. A variable slope method using four parameters was used which does not assume a standard slope, but rather fits the Hill Slope from the data.

2.5 | Enzyme kinetics

Kinetic parameters for D-IRK were determined using a continuous spectrophotometric assay described previously.[14] All experiments (75 μL reactions) were carried out at 30°C in coupled assay buffer containing 100 mM Tris–HCl, pH 7.5, 10 mM $MgCl_2$, 1 mM phosphoenolpyruvate, 0.2 mg/mL NADH, 111 units/mL pyruvate kinase, and 156 units/mL lactate dehydrogenase (Sigma P0924). For determinations of K_m for peptide, reactions contained 500 nM enzyme, 1 mM ATP, and 10–2000 μM of the synthetic peptide substrate KKEEEEYMMMMG.[14,21] For determinations of K_m for ATP, reactions contained 500 nM enzyme, 2 mM peptide, and 100–3000 μM ATP. The activity measured by the slope of NADH oxidation (mOD/min) was plotted against the concentration of ATP and fit the Michaelis–Menten equation using the least square regression method to determine the V_{max} and K_m values of ATP and peptide in GraphPad Prism 9.

2.6 | Autophosphorylation of D-IRK

After concentration and buffer exchange, Ni-NTA purified D-IRK WT was autophosphorylated to the 3P state by incubation with 10 mM ATP and 25 mM $MgCl_2$ for 30–40 min at room temperature. Reactions were quenched with the addition of 25 mM EDTA, centrifuged at 10000 *g* for 10 min, and the protein was analyzed by size exclusion chromatography using a HiLoad Superdex 75 16/600 pg column. Column fractions were analyzed by SDS-PAGE followed by Coomassie staining. Autophosphorylation was verified by native PAGE.

For native PAGE analysis of the phosphorylated forms of D-IRK WT and mutants, autophosphorylation (2–3 μg D-IRK enzyme per lane) was carried out at room temperature in the presence of 2 mM ATP and 2 mM $MgCl_2$ for the indicated time points. In the inhibitor experiment, DMSO or 10 μM linsitinib was added to the enzyme for 10 min at room temperature before the addition of ATP and $MgCl_2$. Reactions were quenched with the addition of a final concentration of 20 mM EDTA, mixed with native gel sample buffer, and run on Biorad miniprotean TGX gels (4561034) for 2–3 h at 100 V. Bands were visualized by Coomassie staining.

2.7 | Fluorescence-based thermal shift assays

The thermal melting temperatures of D-IRK WT and mutant proteins were measured by fluorescence intensities using SYPRO Orange (Sigma S5692). Briefly, enzymes (2 μM) were incubated with DMSO or 10 μM linsitinib in buffer containing 100 mM Tris–HCl, pH 7.5, and 10 mM $MgCl_2$ for 45 min at room temperature, followed by the addition of SYPRO Orange. Triplicate samples in a 96-well plate were heated from 5 to 95°C with a ramp rate of 1% every 2 min in a StepOne Real-Time PCR Machine (Applied Biosystems), during which fluorescence intensities (excitation/emission—470 nm/570 nm) were recorded. Fluorescence intensities were normalized to the maximum and minimum values to obtain relative fluorescence values between 0 and 1. Normalized fluorescent melt curves were fit to a Boltzmann sigmoidal curve in GraphPad Prism 9 to obtain V_{50}. Statistical significance was determined by comparing the means of the mutants to WT using Brown–Forsythe and Welch One-Way ANOVA with corrections for multiple comparisons using Dunnett's T3 multiple comparisons test. Ordinary One-way ANOVA with Šidák correction for multiple comparisons was performed to determine P values comparing the means of linsitinib-treated and the corresponding DMSO-treated controls.

3 | RESULTS

3.1 | *Drosophila* IR kinase purified from a heterologous host is catalytically active

We expressed and purified D-IRK to characterize the kinase activity and substrate specificity. We used the baculovirus expression system to express and purify D-IRK as a His-tagged protein from *Sf*9 insect cells as done previously for human IR/IGF-1R kinases.[20,22] Expression of D-IRK was robust, with purified protein yields up to 8 mg/mL at >95% purity from 1×10^9 insect cells. We carried out size exclusion chromatography to examine whether purified D-IRK formed any multimers or aggregates. D-IRK (39 kD) eluted at fractions corresponded to the monomeric form (Figure 2A). Purified D-IRK is predominantly in its unphosphorylated (0P) form (see below). The triply-phosphorylated (3P) form of D-IRK behaved similarly to the unphosphorylated (0P) form of D-IRK by size exclusion chromatography, indicating that there was no formation of activated D-IRK dimers in solution (Figure S1).

Next, we tested D-IRK activity on a synthetic peptide KKEEEEYMMMMG (hereafter referred to as E4YM4 peptide) that has previously been shown to be an optimal substrate for human IR/IGF-1R kinases in vitro.[14,20,21] This synthetic peptide contains a generic version of the conserved YxxM motifs naturally found in the insulin receptor substrate proteins (IRS1–4) which are dominant substrates for human IR/IGF-1R kinases. D-IRK showed time-dependent phosphorylation of the E4YM4 peptide (Figure 2B). Steady-state kinetic experiments performed with D-IRK using this peptide yielded a K_m (ATP) of 1.35 ± 0.17 mM and a K_m (E4YM4 peptide substrate) of 1.39 ± 0.21 mM (Figure 2C,D). H-IGF-1 RK exhibits a K_m (ATP) of 1.10 mM and K_m (peptide) of 1.40 mM using E4YM4 as a substrate.[16] Kinetic studies with H-IRK have been carried out using poly-(Glu, Tyr) or a peptide derived from the Y939 motif of IRS-1 as substrates. In these studies, H-IRK exhibits a K_m (ATP) ranging from 0.8 to 1.0 mM and K_m (peptide) of ~2 mM.[23–25] Thus, D-IRK enzymatic activity is comparable to H-IGF-1R and IR kinases.

We compared D-IRK activity on E4YM4 with peptides containing recognition motifs for other tyrosine kinases[21,26] (sequences shown in Table 1). These peptides were poor substrates compared to E4YM4 (Figure 3A). D-IRK showed no serine kinase activity on a PKA peptide substrate (Figure 3A), unlike the Ack1 tyrosine kinase.[26] Taken together, these data suggest that D-IRK substrate specificity is similar to its human orthologs.

In contrast to many other tyrosine kinases, the catalytic domains of human IR/IGF-1R kinases are more active in the presence of low concentrations of Mn^{2+}.[27–29] We examined whether D-IRK has similar preferences for divalent cations. D-IRK showed a threefold increase in kinase activity with Mn^{2+} compared to the same concentration of Mg^{2+} (Figure 3B). However, In the presence of both divalent cations, there was no significant difference in the kinase activity compared to Mn^{2+} alone. Thus, Mg^{2+} and Mn^{2+} did not have any additive effects on D-IRK catalytic activity at the concentrations tested.

3.2 | D-IRK exhibits substrate specificity toward particular YxxM motifs of IRS-1 sequences

As mentioned above, IRS proteins are direct substrates for human IR/IGF-1R kinases. IRS proteins are phosphorylated on YxxM motifs, which then act as binding sites for the SH2 domains of the p85 regulatory subunit of PI3K.[30–32] Growth and metabolic effects of IR/IGF-1 R receptors are elicited through IRS phosphorylation and activation of PI3K.[33–36] Human IR/IGF-1R kinases have been shown to phosphorylate several YxxM-containing synthetic IRS-1 peptides with varying specificities.[14,21,29]

CHICO, which is the *Drosophila* homolog of IRS1–4 and a substrate for D-IR, contains two YxxM motifs (Figure 4A) that are potential docking sites for *Drosophila* PI3K.[11] D-IR intracellular domain contains four YxxM motifs, one of which is located in the juxta-membrane region (Figures 1A and 4A).[9,37] D-IR also possesses a carboxyl-terminal extension of ~400 amino acids that is not found in the human IR/IGF-1R kinases or any other vertebrate receptors.[9,12,38] This unique region contains nine tyrosine sites, three of which are present in YxxM/YMxM motifs (Figure 4A). YxxM motifs on CHICO and D-I R facilitate both CHICO-dependent and independent signaling of D-IR kinase.[11,12,18,37]

To investigate whether D-IRK exhibits specificity toward particular YxxM motifs like its human counterparts, we examined D-IRK activity toward four synthetic peptides corresponding to IRS-1 phosphorylation sites (Table 2). The Y939 peptide was the best of these substrates (Figure 4B). Incorporation of phosphate into Y939 was about 2.5-f old higher than Y727 and about 4-fold higher than Y987. The Y895 peptide exhibited equal levels of phosphorylation compared to Y727. However, Y895 does not possess an YxxM motif. Instead, it contains an YxN motif which serves as a consensus sequence for the binding of the SH2 domain of Grb2.[39] It is worth noting that both D-IR and CHICO contain a single YxN motif.[10,11] Synthetic peptides corresponding to the rat β-adrenergic receptor tyrosine phosphorylation sites (not in YxxM or YxN motifs, Table 2)[40,41] were not phosphorylated by D-IRK (Figure 4B).

Our in vitro kinase assays indicate that the substrate preference for D-IRK follows the order of E4YM4 > Y 939 > Y727 = Y895 > Y987 (Figures 3A and 4B), which was

different from H-IRK (Figure 4C). H-I RK preferred the YxN-containing Y895 over the YxxM-containing Y939. However, our H-IRK construct contains the juxta-membrane region which may have influenced the substrate specificities shown in Figure 4C.[22,42] The E4YM4 and Y939 peptides contain two acidic residues N-terminal to the phosphorylatable tyrosines compared to just one in the Y727 and Y897 peptides (Tables 1 and 2). Our data indicate that the presence of an additional acidic residue may play an important role in directing the activity of D-IRK beyond the influence of the YxxM motif.

3.3 | D-IRK activity is inhibited by linsitinib

Linsitinib (OSI-906) is a selective and potent inhibitor of human IR/IGF-1R kinases.[43,44] We therefore investigated whether D-IRK activity can be inhibited by linsitinib (Figure 5A). We also tested the efficacy of a panel of other FDA-approved tyrosine kinase inhibitors and the non-specific kinase inhibitor staurosporine against D-IRK and H-IRK (Figure 5A,B). Linsitinib at 10 μM inhibited the activity of D-IRK by 98% compared to 85% for H-IR kinase activity (Figure 5B). Vandetanib, a VEGFR/EGFR/RET receptor tyrosine kinase inhibitor, and dasatinib, a Src/Abl inhibitor, inhibited D-I RK activity by about 70% and 50%, respectively, with similar effects on H-IRK. The EGFR-specific inhibitors lapatinib and erlotinib showed marginal inhibition of D-IRK activity (by about 10% each), and were more effective against H-IRK (43% and 35%, respectively) (Figure 5B). As expected, the broad-spectrum protein kinase inhibitor staurosporine also blocked the D-IRK activity, by 98% at 10 μM (Figure 5A). Our data indicate that linsitinib is a potent inhibitor of both D-IRK and H-IRK, and that EGFR inhibitors are more effective against H-IRK than D-IRK.

Linsitinib demonstrates greater potency against H-IGF-1R than H-IR (the value of IC_{50} for H-IGF-1R is 35 nM, vs. 75 nM for H-IR).[43] We determined that the half-maximal inhibitory concentration (IC_{50}) of linsitinib against D-IRK was 38.6 nM (Figure 5C). Activation of human IR/IGF-1R kinases takes place with the stepwise phosphorylation of the three tyrosines in the activation loop wherein the enzyme transitions from the basal 0P state to the fully activated 3P state.[14–16,45] Linsitinib is an ATP-competitive inhibitor that blocks autophosphorylation to inhibit the intrinsic tyrosine kinase activity of human IR/IGF-1R kinases.[43] To verify the mechanism of inhibition of D-IRK, we analyzed autophosphorylation reactions by native PAGE with and without linsitinib. In the absence of linsitinib, D-IRK progressed from the 0P form to 1P, 2P, and 3P forms in 10 min. In contrast, the addition of linsitinib prevented the transition of D-IRK from 0P to 1P, indicating that linsitinib blocked autophosphorylation of D-IRK (shown in Figure 5D).

3.4 | D-IRK mutations associated with *Drosophila* development and lifespan have varying effects on kinase activities and protein stability

D-IR plays a crucial role in regulating growth, metabolism, and development in *Drosophila*.[6,10,11,46,47] Like the *C. elegans* counterpart, *Daf-2*, impaired D-IR signaling is associated with extended longevity.[3,6,10,48] The R1467C (numbering according to NCBI NP_524436.2) mutation in the kinase insert region is associated with a reduction in head size,[6] body size, and a drastic increase in life expectancy of fruit flies.[10] With varying degrees of severity, similar effects are seen with the G1599R mutation in the C-lobe[6,10] and the I1544F mutation in the activation loop of D-IRK.[10] It is important to realize that the

phenotypic effects of these mutations on fruit fly physiology are studied in the context of site-specific mutations[6] or as heterozygous alleles,[10] as homozygous null mutations in fruit flies are lethal.

We generated mutations in the D-IRK corresponding to the alleles that regulate growth, development, and life expectancy in *Drosophila* (shown in Table 3 and *Top*, Figure 6A). We expressed and purified the mutant kinases from *Sf*9 insect cells to investigate the direct effects of these mutations on kinase activity (*Bottom*, Figure 6A). The D-IRK R1467C and G1599R mutations showed partial losses of kinase activity toward the E4YM4 peptide substrate as compared to wild-type D-IRK (WT) (*Bottom*, Figure 6A). D-IRK I1544F mutation showed no significant change in kinase activity compared to WT, suggesting that the impact of D-IRK I1544F mutation on *Drosophila* longevity[10] may not be related to the kinase activity per se. D-IR contains an extra 12 amino acids in the kinase insert domain (residues 1476–1487) relative to H-IR kinase, bearing a YxN motif. We also generated a mutant D-IRK with this portion deleted (annotated as ΔKI) and examined kinase activity. The kinase activity of D-IRK ΔKI was comparable to WT (*Bottom*, Figure 6A), suggesting that this segment of the kinase is non-essential for catalytic activity. All mutant kinases progressed from 0P to 3P autophosphorylated states that were comparable to WT within the 15-min time period (Figure 6B), suggesting that the D-IRK R1467C and G1599R mutations may affect catalytic activity toward exogenous substrates, rather than autophosphorylation.

To characterize the catalytic activity of D-IRK R1467C and G1599R mutations, we determined their kinetic constants V_{max} and K_m for ATP against the E4YM4 peptide substrate. The V_{max} values for both D-IRK R1467C (58.43 mOD/min) and G1599R (67.5 mOD/min) were about 50% lower than WT (120.9 mOD/min) (Figures 2C and 7A,B). D-IRK R1467C (1.55 mM ATP) showed a marginal increase (14.8%), whereas D-IRK G1599R (1.86 mM ATP) had a greater increase (37.7%) in K_m for ATP compared to WT (1.35 mM ATP) (Figures 2C and 7A,B).

Missense mutations can alter thermal stability of protein kinases and consequently impair their catalytic activities.[49,50] We therefore compared the thermodynamic stabilities by measuring the melting temperatures (T_m) of WT and mutant D-IRK using fluorescence-based thermal shift assays.[51] For this, the D-IRKs were subjected to increasing temperatures, and protein denaturation was monitored using SYPRO Orange dye. This dye preferentially binds to the hydrophobic regions on the proteins which are increasingly exposed during denaturation. T_m was determined as the mid-point of the thermal denaturation curve[52] (Figure 8A,C).

The mean T_m values of D-IRK R1467C, G1599R, and ΔKI were lower than WT (Figure 8B). The decrease in the T_m for D-IRK ΔKI is likely due to the removal of 12 amino acids in the kinase insert region, although that did not affect its kinase activity. The lower mean T_m values of D-IRK R1467C and G1599R indicate weakened stability of these mutants, which may have contributed to their reduced catalytic activities. In contrast, the I1544F mutation did not affect the T_m of D-IRK.

Ligands including kinase inhibitors can promote protein stability and increase T_m.[51,53] To examine whether the D-IRK mutations interfere with linsitinib binding, we carried out thermal shift assays in the presence of linsitinib. The addition of linsitinib led to an increase in the T_m for the WT and all the mutant D-IRKs (Figure 8D). Our data indicate that the D-IRK mutations located away from the ATP-binding pocket did not alter the integrity of the ATP-binding site, as linsitinib binding remained unaffected.

4 | DISCUSSION

Peptide libraries containing randomized residues adjacent to the phosphorylatable tyrosine have been used to determine substrate specificities of various tyrosine kinases.[21,54–56] For H-IR, these studies resulted in the identification of the E4YM4 sequence as an efficient peptide substrate. D-IRK exhibited strong catalytic activity against several peptide substrates, and like its human counterpart phosphorylated peptides with YxxM motifs. Overall, D-IRK behaved similarly to H-IRK in terms of substrate phosphorylation and inhibition to linsitinib.

Although all our YxxM peptides contained at least one negatively charged residue N-terminus to the target tyrosine, peptides with two acidic residues in the −1 and − 2 positions relative to the target tyrosine were the best substrates. It is interesting to note that all four YxxM motifs located in the intracellular domain of D-IR *do not* contain acidic residues at the −1 and − 2 positions N-terminal to the target tyrosine (Figure 9A). The presence of these YxxM motifs on the same polypeptide as D-IR (as opposed to being present on synthetic peptides, as in our study) would be expected to increase the efficiency of their phosphorylation. On the other hand, *both* YxxM motifs in CHICO contain two acidic residues in the −2 and − 3 positions (Figure 9B), presumably because phosphorylation of these motifs is dependent on D-IR-CHICO binding. The presence of CHICO-independent signaling through D-IR, facilitated by its C-terminal extension, has been observed to influence cell growth and survival.[18,37] Cell-specific proteolytic cleavage of the C-terminal end of D-IR[9] may function as an additional level of targeted signaling via CHICO.

Activation of H-I R involves the trans-autophosphorylation of intracellular tyrosine residues in the juxta-membrane region (Y972), activation loop (Y1158, Y1162, and Y1163), and the C-terminal domain (Y1328 and Y1334). The structural changes that induce trans-autophosphorylation of H-IR kinase domains originate with the binding of insulin, triggering a shift of the third fibronectin type III domains (FnIII-3) toward each other as evidenced by cryo-EM structures.[57,58] A recent cryo-E M structure of the extracellular domain of D-IR bound to *Drosophila* insulin-like peptide 5 (DILP5) indicates similar overall arrangements of the FnIII-3 domains as in insulin bound H-IR.[59] D-IR-specific loops in the FnIII domains provide additional stability for the DILP5 interaction; these modifications in the D-IR extracellular domain may stabilize the receptor–ligand complex during DILP activation, allowing for distal autophosphorylation of the C-termini YxxM motifs.

The intracellular domain of D-IR contains multiple tyrosines arranged in motifs that serve as potential recognition sites for proteins containing SH2 and phosphotyrosine binding (PTB) domains.[30,31,39,60–62] These motifs consist of five NPxY, four YxxM, two each of YxxL and

YxxP, and one YxN.[9,37] Notably, all four tyrosines within the YxxM motifs (Y1354, Y1989, Y2005, and Y2026) and one tyrosine in an YxxL motif (Y1965) are also part of a highly conserved NPNY motif (Figure 9A). However, the molecular relevance of these motifs in the D-IR-signaling pathway is not well understood.

In humans, the NPxY motif in IR/IGF-1R functions as a docking site for PTB domain-containing proteins such as IRS-1.[60] In the NPxY motif of H-IR, a leucine residue at the −8 position and a serine residue at the −5 position (relative to the phosphorylated tyrosine) are important for high affinity and preferential binding of IRS-1 to H-IR.[63] The juxta-membrane NPFY in D-IR lacks a serine at the −5 position. However, the NPNY motifs in the D-IR C-terminal domain contain a conserved serine at this position relative to the target tyrosine (shown in Figure 9A). Unlike the juxta-membrane domain, these C-terminal motifs play a crucial role in establishing stable associations with CHICO, as mutations of the juxta-membrane NPxY diminish D-IR's ability to phosphorylate CHICO.[64] The NPxY motifs in the D-IR intracellular domain also lack a leucine at the −8 position. Amino acids at the −1 position in NPxY motifs are known to selectively modulate affinities with various PTB-containing proteins.[61,65] Indeed, the amino acid in the −1 position is different in the D-IR juxta-membrane and C-terminal NPxY sequences. These observations suggest that the conserved SxNPNYxxM repeats in the C-terminal domain of D-IR may play an important role in signaling specificity. It is conceivable that, depending on the cellular context and the DILP type, D-IR may utilize NPxY motifs for PTB-containing proteins such as CHICO or YxxM motifs for SH2-containing proteins such as PI3K.

Drosophila is a holometabolous insect and undergoes complete metamorphosis to develop from embryo to adult via larval and pupal stages. These developmental stages are accompanied by changes in physiological pH and osmotic pressures,[66,67] which may impact signaling mechanisms. Responses to environmental factors involve the intersection of many pathways. In *Drosophila*, the insulin and TOR pathways closely regulate growth and lifespan.[68,69] pH and osmotic pressure variation may influence factors upstream of D-IR that can impact the strength and specificity of D-IRK signaling. This study focused solely on the catalytic action of D-IRK, excluding the influence of other regulatory factors and pathways. Exploring how these physiological changes could impact D-IR signaling will be an important avenue for future investigations.

We generated D-IRK mutations that correspond to alleles linked to growth, development, and longevity. Using kinetic assays, we uncovered varying effects of these mutations on kinase activity and stability. Mutations R1467C and G1599R exhibited reduced kinase activity and thermal stability. In line with their longevity-associated effects, the R1467C and G1599R mutations displayed altered kinetic properties with lowered maximal velocities, suggesting that they could reduce D-IR activity in cellular-signaling pathways. Addition of linsitinib increased the thermal stability of WT and mutant D-IRK, indicating that these mutations did not have any major effects on the ATP-binding pocket. The increased longevity[10] and decreased head size[6] phenotypes in *Drosophila* due to the R1467C and G1599R mutations may be attributed to the inefficient catalytic capabilities of these mutant kinases independent of other D-IR regulatory regions. In humans, a homozygous R1092E mutation (analogous to the R1467 residue in *Drosophila*) causes a severe form

of leprechaunism known as Donohue Syndrome, which is characterized by severe growth retardation, insulin resistance, and low viability.[70]

Interestingly, although the I1544F mutation is proximal to the activating tyrosines in the activation loop, we found that it had no impact on kinase activity or thermal stability, suggesting that the longevity effects observed in fruit flies[10] may be related to other factors such as impaired substrate recruitment, effects of other regulatory regions in D-IR, and/or a result of synergistic effects with other D-IR mutations. Furthermore, we found that deleting the extra 12 amino acids in the kinase insert region of D-IRK also did not impact kinase activity. The fact that this region contains a YxN motif that can potentially recruit the SH2 domain-containing Grb2 suggests that this portion of the D-IRK could be more important for substrate recruitment than for catalysis.

The growth, fecundity, and longevity effects of D-IR R1467C (InR^{353} allele), I1544F (InR^{74} allele), and G1599R (InR^{211} allele) mutations are only observed when heterozygous with WT or other D-IR mutations (such as the InR^{E19} allele). Homozygous null mutations of R1467C, I1544F, and G1599R are lethal to fruit flies,[10] which impedes our ability to fully understand the physiological effects of these mutations. Our data show that R1467C and G1599R mutations did not completely abrogate kinase activities. Thus, partial loss of function is sufficient to elicit a phenotype in heterozygous fruit flies. Patients heterozygous for the human R1092E mutation have mild or moderate reduction in H-IR kinase activities and do not show the severe defects of leprechaunism that is seen in homozygous condition, but instead have type A insulin resistance.[70]

The highly conserved insulin receptor-signaling pathway in *Drosophila melanogaster* has facilitated numerous genetic investigations aimed at unraveling the significance of the D-IR pathway in growth, metabolism, and lifespan. As a result, *Drosophila* has emerged as a pertinent model system for comprehending human conditions such as diabetes and aging. Robust expression of D-IRKs from a heterologous host enabled our biochemical studies to elucidate catalytic activity, substrate specificity, and response to kinase inhibitors. Our findings provide new perspectives on how particular residues and segments within D-IRK influence its inherent function and provide a platform for interrogating additional D-IR mutants that are involved in regulation of growth, development, and longevity.

Supplementary Material

Refer to Web version on PubMed Central for supplementary material.

ACKNOWLEDGMENTS

We thank Barbara Craddock for maintaining stock cultures of *Sf9* cells and Stephen J. Collins for helpful recommendations on inhibitor assays. This work was funded by Veterans Administration Merit Award I01BX006248 to W.T.M.

Funding information

Veterans Administration Merit Award, Grant/Award Number: I01 BX006248

DATA AVAILABILITY STATEMENT

Included in article. All data that support the findings of this study are available in the Materials and Methods section of this article. Any research material used in this study may be requested from the corresponding author of this manuscript.

Abbreviations:

DILP	Drosophila insulin-like peptide
D-IR	Drosophila insulin receptor
D-IRK	D-IR kinase domain
H-IR	human insulin receptor
IGF-1R	insulin-like growth factor 1 receptor
IIS	insulin/IGF-1 signaling
IR	insulin receptor
IRS	insulin receptor substrate
PI3K	phosphatidylinositol 3′-kinase
PTB	phosphotyrosine binding
SH2	Src homology 2
Tm	melting temperature
WT	wild-type

REFERENCES

1. Venz R, Pekec T, Katic I, Ciosk R, Ewald CY. End-of-life targeted degradation of DAF-2 insulin/IGF-1 receptor promotes longevity free from growth-related pathologies. Elife. 2021;10:e71335. [PubMed: 34505574]
2. Vitale G, Pellegrino G, Vollery M, Hofland LJ. ROLE of IGF-1 system in the modulation of longevity: controversies and new insights from a Centenarians' perspective. Front Endocrinol (Lausanne). 2019;10:27. [PubMed: 30774624]
3. Clancy DJ, Gems D, Harshman LG, et al. Extension of life-span by loss of CHICO, a Drosophila insulin receptor substrate protein. Science. 2001;292:104–106. [PubMed: 11292874]
4. Garofalo RS. Genetic analysis of insulin signaling in Drosophila. Trends Endocrinol Metab. 2002;13:156–162. [PubMed: 11943559]
5. Barbieri M, Bonafe M, Franceschi C, Paolisso G. Insulin/IGF-I-signaling pathway: an evolutionarily conserved mechanism of longevity from yeast to humans. Am J Physiol Endocrinol Metab. 2003;285:E1064–E1071. [PubMed: 14534077]
6. Brogiolo W, Stocker H, Ikeya T, Rintelen F, Fernandez R, Hafen E. An evolutionarily conserved function of the Drosophila insulin receptor and insulin-like peptides in growth control. Curr Biol. 2001;11:213–221. [PubMed: 11250149]
7. Slaidina M, Delanoue R, Gronke S, Partridge L, Leopold P. A Drosophila insulin-like peptide promotes growth during nonfeeding states. Dev Cell. 2009;17:874–884. [PubMed: 20059956]

8. Sajid W, Kulahin N, Schluckebier G, et al. Structural and biological properties of the Drosophila insulin-like peptide 5 show evolutionary conservation. J Biol Chem. 2011;286:661–673. [PubMed: 20974844]
9. Fernandez R, Tabarini D, Azpiazu N, Frasch M, Schlessinger J. The Drosophila insulin receptor homolog: a gene essential for embryonic development encodes two receptor isoforms with different signaling potential. EMBO J. 1995;14:3373–3384. [PubMed: 7628438]
10. Yamamoto R, Palmer M, Koski H, Curtis-Joseph N, Tatar M. Aging modulated by the Drosophila insulin receptor through distinct structure-defined mechanisms. Genetics. 2021;217:iyaa037. [PubMed: 33724413]
11. Bohni R, Riesgo-Escovar J, Oldham S, et al. Autonomous control of cell and organ size by CHICO, a Drosophila homolog of vertebrate IRS1–4. Cell. 1999;97:865–875. [PubMed: 10399915]
12. Yenush L, Fernandez R, Myers MG Jr, et al. The Drosophila insulin receptor activates multiple signaling pathways but requires insulin receptor substrate proteins for DNA synthesis. Mol Cell Biol. 1996;16:2509–2517. [PubMed: 8628319]
13. Ebina Y, Ellis L, Jarnagin K, et al. The human insulin receptor cDNA: the structural basis for hormone-activated transmembrane signalling. Cell. 1985;40:747–758. [PubMed: 2859121]
14. Favelyukis S, Till JH, Hubbard SR, Miller WT. Structure and autoregulation of the insulin-like growth factor 1 receptor kinase. Nat Struct Biol. 2001;8:1058–1063. [PubMed: 11694888]
15. Hubbard SR. Crystal structure of the activated insulin receptor tyrosine kinase in complex with peptide substrate and ATP analog. EMBO J. 1997;16:5572–5581. [PubMed: 9312016]
16. Li W, Miller WT. Role of the activation loop tyrosines in regulation of the insulin-like growth factor I receptor-tyrosine kinase. J Biol Chem. 2006;281:23785–23791. [PubMed: 16793764]
17. Jumper J, Evans R, Pritzel A, et al. Highly accurate protein structure prediction with AlphaFold. Nature. 2021;596:583–589. [PubMed: 34265844]
18. Li CR, Guo D, Pick L. Independent signaling by Drosophila insulin receptor for axon guidance and growth. Front Physiol. 2013;4:385. [PubMed: 24478707]
19. Chen C, Jack J, Garofalo RS. The Drosophila insulin receptor is required for normal growth. Endocrinology. 1996;137:846–856. [PubMed: 8603594]
20. Cabail MZ, Li S, Lemmon E, Bowen ME, Hubbard SR, Miller WT. The insulin and IGF1 receptor kinase domains are functional dimers in the activated state. Nat Commun. 2015;6:6406. [PubMed: 25758790]
21. Songyang Z, Carraway KL 3rd, Eck MJ, et al. Catalytic specificity of protein-tyrosine kinases is critical for selective signalling. Nature. 1995;373:536–539. [PubMed: 7845468]
22. Craddock BP, Cotter C, Miller WT. Autoinhibition of the insulin-like growth factor I receptor by the juxtamembrane region. FEBS Lett. 2007;581:3235–3240. [PubMed: 17586502]
23. Ablooglu AJ, Kohanski RA. Activation of the insulin receptor's kinase domain changes the rate-determining step of substrate phosphorylation. Biochemistry. 2001;40:504–513. [PubMed: 11148045]
24. Frankel M, Ablooglu AJ, Leone JW, et al. Intrasteric inhibition of ATP binding is not required to prevent unregulated autophosphorylation or signaling by the insulin receptor. Mol Cell Biol. 2001;21:4197–4207. [PubMed: 11390649]
25. Li S, Covino ND, Stein EG, Till JH, Hubbard SR. Structural and biochemical evidence for an autoinhibitory role for tyrosine 984 in the juxtamembrane region of the insulin receptor. J Biol Chem. 2003;278:26007–26014. [PubMed: 12707268]
26. Yokoyama N, Lougheed J, Miller WT. Phosphorylation of WASP by the Cdc42-associated kinase ACK1: dual hydroxyamino acid specificity in a tyrosine kinase. J Biol Chem. 2005;280:42219–42226. [PubMed: 16257963]
27. Kwok YC, Nemenoff RA, Powers AC, Avruch J. Kinetic properties of the insulin receptor tyrosine protein kinase: activation through an insulin-stimulated tyrosine-specific, intramolecular autophosphorylation. Arch Biochem Biophys. 1986;244:102–113. [PubMed: 3004334]
28. Mothe I, Tartare S, Kowalski-Chauvel A, Kaliman P, Van Obberghen E, Ballotti R. Tyrosine kinase activity of a chimeric insulin-like-growth-factor-1 receptor containing the insulin receptor C-terminal domain. Comparison with the tyrosine kinase activities of the insulin and insulin-like-

growth-factor-1 receptors using a cell-free system. Eur J Biochem. 1995;228:842–848. [PubMed: 7737184]

29. Xu B, Bird VG, Miller WT. Substrate specificities of the insulin and insulin-like growth factor 1 receptor tyrosine kinase catalytic domains. J Biol Chem. 1995;270:29825–29830. [PubMed: 8530377]
30. Backer JM, Myers MG Jr, Shoelson SE, et al. Phosphatidylinositol 3′-kinase is activated by association with IRS-1 during insulin stimulation. EMBO J. 1992;11:3469–3479. [PubMed: 1380456]
31. Songyang Z, Shoelson SE, Chaudhuri M, et al. SH2 domains recognize specific phosphopeptide sequences. Cell. 1993;72:767–778. [PubMed: 7680959]
32. Thorpe LM, Yuzugullu H, Zhao JJ. PI3K in cancer: divergent roles of isoforms, modes of activation and therapeutic targeting. Nat Rev Cancer. 2015;15:7–24. [PubMed: 25533673]
33. Jones JI, Clemmons DR. Insulin-like growth factors and their binding proteins: biological actions. Endocr Rev. 1995;16:3–34. [PubMed: 7758431]
34. Rordorf-Nikolic T, Van Horn DJ, Chen D, White MF, Backer JM. Regulation of phosphatidylinositol 3′-kinase by tyrosyl phosphoproteins. Full activation requires occupancy of both SH2 domains in the 85-kDa regulatory subunit. J Biol Chem. 1995;270:3662–3666. [PubMed: 7876105]
35. Uchida T, Myers MG Jr, White MF. IRS-4 mediates protein kinase B signaling during insulin stimulation without promoting antiapoptosis. Mol Cell Biol. 2000;20:126–138. [PubMed: 10594015]
36. Esposito DL, Li Y, Cama A, Quon MJ. Tyr(612) and Tyr(632) in human insulin receptor substrate-1 are important for full activation of insulin-stimulated phosphatidylinositol 3-kinase activity and translocation of GLUT4 in adipose cells. Endocrinology. 2001;142:2833–2840. [PubMed: 11416002]
37. Marin-Hincapie M, Garofalo RS. The carboxyl terminal extension of the Drosophila insulin receptor homologue binds IRS-1 and influences cell survival. J Biol Chem. 1999;274:24987–24994. [PubMed: 10455177]
38. Ruan Y, Chen C, Cao Y, Garofalo RS. The Drosophila insulin receptor contains a novel carboxyl-terminal extension likely to play an important role in signal transduction. J Biol Chem. 1995;270:4236–4243. [PubMed: 7876183]
39. Sun XJ, Crimmins DL, Myers MG Jr, Miralpeix M, White MF. Pleiotropic insulin signals are engaged by multisite phosphorylation of IRS-1. Mol Cell Biol. 1993;13:7418–7428. [PubMed: 7504175]
40. Baltensperger K, Karoor V, Paul H, Ruoho A, Czech MP, Malbon CC. The beta-adrenergic receptor is a substrate for the insulin receptor tyrosine kinase. J Biol Chem. 1996;271:1061–1064. [PubMed: 8557631]
41. Doronin S, Lin F, Wang HY, Malbon CC. The full-length, cytoplasmic C-terminus of the beta 2-adrenergic receptor expressed in E. Coli acts as a substrate for phosphorylation by protein kinase a, insulin receptor tyrosine kinase, GRK2, but not protein kinase C and suppresses desensitization when expressed in vivo. Protein Expr Purif. 2000;20:451–461. [PubMed: 11087685]
42. Cann AD, Bishop SM, Ablooglu AJ, Kohanski RA. Partial activation of the insulin receptor kinase domain by juxtamembrane autophosphorylation. Biochemistry. 1998;37:11289–11300. [PubMed: 9698376]
43. Mulvihill MJ, Cooke A, Rosenfeld-Franklin M, et al. Discovery of OSI-906: a selective and orally efficacious dual inhibitor of the IGF-1 receptor and insulin receptor. Future Med Chem. 2009;1:1153–1171. [PubMed: 21425998]
44. McKinley ET, Bugaj JE, Zhao P, et al. 18FDG-PET predicts pharmacodynamic response to OSI-906, a dual IGF-1R/IR inhibitor, in preclinical mouse models of lung cancer. Clin Cancer Res. 2011;17:3332–3340. [PubMed: 21257723]
45. Hubbard SR. The insulin receptor: both a prototypical and atypical receptor tyrosine kinase. Cold Spring Harb Perspect Biol. 2013;5:a008946. [PubMed: 23457259]

46. Palermo J, Keene AC, DiAngelo JR. Expression of a constitutively active insulin receptor in drosulfakinin (Dsk) neurons regulates metabolism and sleep in Drosophila. Biochem Biophys Rep. 2022;30:101280. [PubMed: 35600902]
47. Banzai K, Nishimura T. Isolation of a novel missense mutation in insulin receptor as a spontaneous revertant in ImpL2 mutants in Drosophila. Development. 2023;150:dev201248. [PubMed: 36504086]
48. Tatar M, Kopelman A, Epstein D, Tu MP, Yin CM, Garofalo RS. A mutant Drosophila insulin receptor homolog that extends life-span and impairs neuroendocrine function. Science. 2001;292:107–110. [PubMed: 11292875]
49. Lori C, Lantella A, Pasquo A, et al. Effect of single amino acid substitution observed in cancer on Pim-1 kinase thermodynamic stability and structure. PloS One. 2013;8:e64824. [PubMed: 23755147]
50. Novak L, Petrosino M, Pasquo A, et al. Mutation in the common docking domain affects MAP kinase ERK2 catalysis and stability. Cancers (Basel). 2023;15:2938. [PubMed: 37296900]
51. Niesen FH, Berglund H, Vedadi M. The use of differential scanning fluorimetry to detect ligand interactions that promote protein stability. Nat Protoc. 2007;2:2212–2221. [PubMed: 17853878]
52. Huynh K, Partch CL. Analysis of protein stability and ligand interactions by thermal shift assay. Curr Protoc Protein Sci. 2015;79:28.29.1–28.29.14.
53. Krishna SN, Luan CH, Mishra RK, et al. A fluorescence-based thermal shift assay identifies inhibitors of mitogen activated protein kinase 4. PloS One. 2013;8:e81504. [PubMed: 24339940]
54. Chan PM, Keller PR, Connors RW, Leopold WR, Miller WT. Amino-terminal sequence determinants for substrate recognition by platelet-derived growth factor receptor tyrosine kinase. FEBS Lett. 1996;394:121–125. [PubMed: 8843147]
55. Shoelson SE, Chatterjee S, Chaudhuri M, White MF. YMXM motifs of IRS-1 define substrate specificity of the insulin receptor kinase. Proc Natl Acad Sci U S A. 1992;89:2027–2031. [PubMed: 1312712]
56. Trinh TB, Xiao Q, Pei D. Profiling the substrate specificity of protein kinases by on-bead screening of peptide libraries. Biochemistry. 2013;52:5645–5655. [PubMed: 23848432]
57. Weis F, Menting JG, Margetts MB, et al. The signalling conformation of the insulin receptor ectodomain. Nat Commun. 2018;9:4420. [PubMed: 30356040]
58. Gutmann T, Kim KH, Grzybek M, Walz T, Coskun U. Visualization of ligand-induced transmembrane signaling in the full-length human insulin receptor. J Cell Biol. 2018;217:1643–1649. [PubMed: 29453311]
59. Viola CM, Frittmann O, Jenkins HT, Shafi T, De Meyts P, Brzozowski AM. Structural conservation of insulin/IGF signalling axis at the insulin receptors level in Drosophila and humans. Nat Commun. 2023;14:6271. [PubMed: 37805602]
60. Kaburagi Y, Yamamoto-Honda R, Tobe K, et al. The role of the NPXY motif in the insulin receptor in tyrosine phosphorylation of insulin receptor substrate-1 and Shc. Endocrinology. 1995;136:3437–3443. [PubMed: 7543044]
61. Wolf G, Trub T, Ottinger E, et al. PTB domains of IRS-1 and Shc have distinct but overlapping binding specificities. J Biol Chem. 1995;270:27407–27410. [PubMed: 7499194]
62. Liu BA, Engelmann BW, Nash PD. The language of SH2 domain interactions defines phosphotyrosine-mediated signal transduction. FEBS Lett. 2012;586:2597–2605. [PubMed: 22569091]
63. Eck MJ, Dhe-Paganon S, Trub T, Nolte RT, Shoelson SE. Structure of the IRS-1 PTB domain bound to the juxtamembrane region of the insulin receptor. Cell. 1996;85:695–705. [PubMed: 8646778]
64. Poltilove RM, Jacobs AR, Haft CR, Xu P, Taylor SI. Characterization of Drosophila insulin receptor substrate. J Biol Chem. 2000;275:23346–23354. [PubMed: 10801879]
65. Trub T, Choi WE, Wolf G, et al. Specificity of the PTB domain of Shc for beta turn-forming pentapeptide motifs amino-terminal to phosphotyrosine. J Biol Chem. 1995;270:18205–18208. [PubMed: 7543098]
66. Massie HR, Williams TR, Colacicco JR. Changes in pH with age in Drosophila and the influence of buffers on longevity. Mech Ageing Dev. 1981;16:221–231. [PubMed: 6792427]

67. Riedl CA, Oster S, Busto M, Mackay TF, Sokolowski MB. Natural variability in Drosophila larval and pupal NaCl tolerance. J Insect Physiol. 2016;88:15–23. [PubMed: 26874056]

68. Kapahi P, Zid BM, Harper T, Koslover D, Sapin V, Benzer S. Regulation of lifespan in Drosophila by modulation of genes in the TOR signaling pathway. Curr Biol. 2004;14:885–890. [PubMed: 15186745]

69. Partridge L, Alic N, Bjedov I, Piper MD. Ageing in Drosophila: the role of the insulin/Igf and TOR signalling network. Exp Gerontol. 2011;46:376–381. [PubMed: 20849947]

70. Takahashi Y, Kadowaki H, Momomura K, et al. A homozygous kinase-defective mutation in the insulin receptor gene in a patient with leprechaunism. Diabetologia. 1997;40:412–420. [PubMed: 9112018]

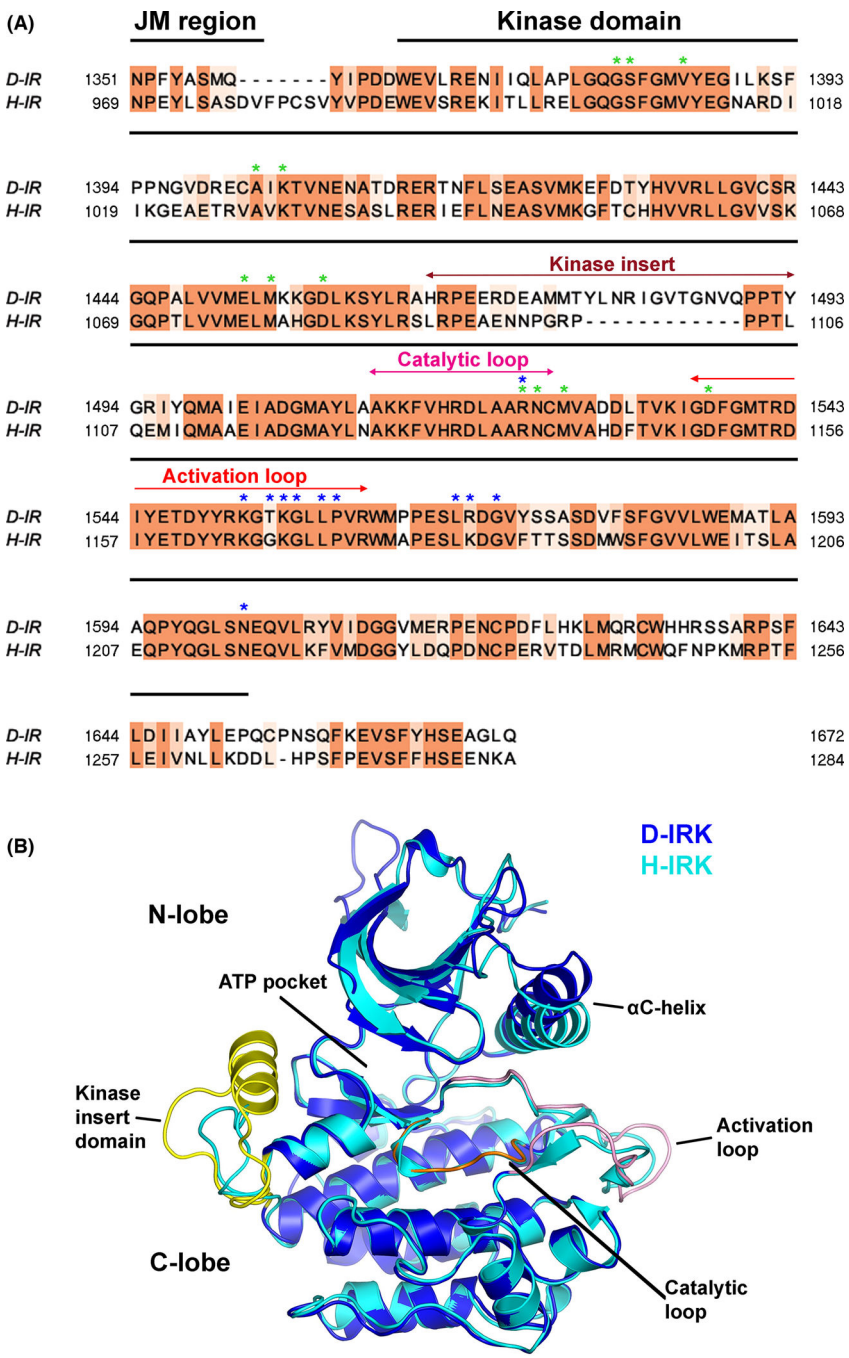

FIGURE 1.

D-IRK is homologous to H-IRK. (A) Sequence alignment of D-IRK and H-IRK shows ~60% identity in this region. D-IRK residues 1351–1672 (NCBI Reference Sequence: NP_524436.2) encompassing a portion of the juxta-membrane region and the entire kinase domain was aligned with the H-IRK residues 969–1284 (numbering according to Ebina et al.[13]) using the MUSCLE multiple sequence alignment tool. Aligned sequences were visualized and color-coded in Jalview, and manually annotated. The darker columns represent the alignment of identical amino acid residues, whereas the lighter colors represent

the alignment of less conserved positions. Amino acid residues participating in ATP binding are indicated by green asterisks and peptide substrate binding by blue asterisks. Maroon double arrow indicates the kinase insert region, magenta is the catalytic loop region with the HRD motif, and red is the activation loop containing the DFG motif and the three-activating tyrosine autophosphorylation sites. (B) Superimposition of the predicted active form of D-IRK in blue (AlphaFold: AF-P09208-F1, residues 1362–1672 corresponding to NCBI NP_524436.2) with the active form of H-IRK in cyan (PDB: 1IR3, residues 987–1283) showing various structural elements including the five β-sheets in the N-lobe, αC-helix, ATP-binding pocket, activation loop (colored pink D-IRK), kinase insert domain (colored yellow in D-IRK), and catalytic domain (colored orange in D-IRK). Models were generated in PyMOL and then manually annotated.

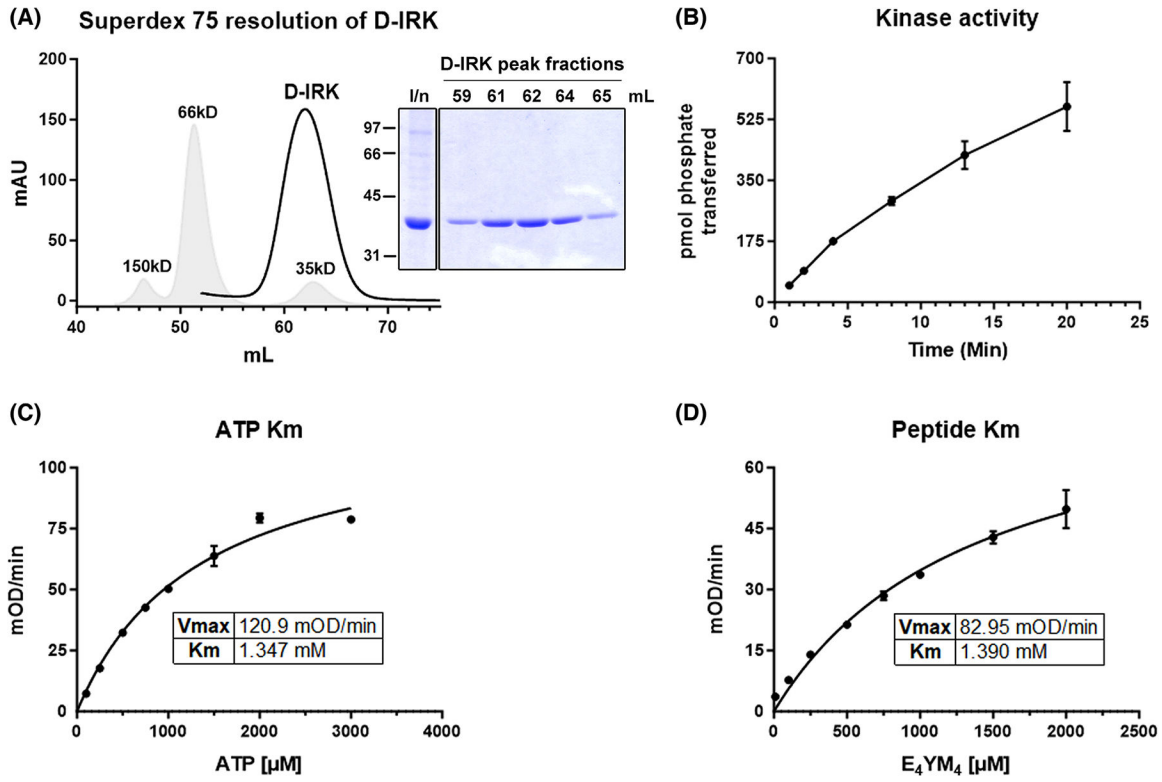

FIGURE 2.

D-IRK purifies as a monomer and is catalytically active in vitro. (A) *Left* Ni-NTA purified D-IRK was resolved in a HiLoad Superdex 75 16/600 pg column attached to an ÄKTA Pure 25 chromatography system. D-IRK (39 kD) eluted at fractions that corresponds to the monomeric form. Elution peaks of standard proteins at various molecular weights are indicated in gray. *Right* Ni-NTA purified D-IRK (I/n, Superdex 75 input) and D-IRK peak fractions at 59–65 mL elution from the Superdex 75 purification were run on SDS-PAGE gel and visualized by Coomassie staining. (B) Kinase activity of Ni-NTA purified D-IRK (0.5 μM) was measured using the phosphocellulose paper-binding assays with [γ^{-32} P]-ATP and is indicated as pmol of phosphate transferred to KKEEEEYMMMMG (E4YM4) peptide substrate (0.5 mM) at various time points. (C and D) Continuous spectrophotometric assays were performed to determine the kinetic constants of D-IRK using 0.5 μM enzyme reactions in duplicates. (C) For ATP K_m, 2 mM of E4YM4 peptide substrate and 100–3000 μM ATP were used. (D) For peptide K_m, 1 mM ATP and 10–2000 μM of E4YM4 peptide substrate were used. V_{max} and K_m for ATP or peptide were derived from fitting the slopes of NADH oxidation (mOD/min) plotted against the ATP or peptide concentrations, to the Michaelis–Menten equation.

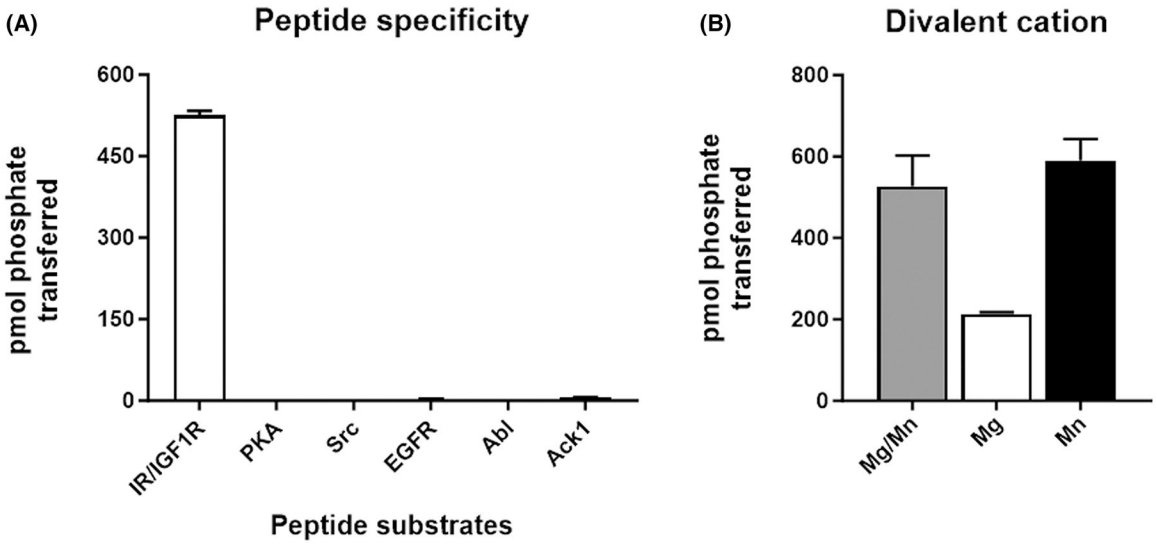

FIGURE 3.

Purified D-IRK behaves similarly to H-IRK/IGF-1RK. Phosphorylation of synthetic peptides (0.5 mM) (sequences shown in Table 1) by Ni-NTA purified D-IRK (0.5 μM) was measured using the phosphocellulose paper-binding assay with [$\gamma-^{32}$ P]-ATP. Kinase activity is indicated as picomoles (pmol) of phosphate transferred onto the peptide substrates. Figures are a representative of two independent experiments each performed in duplicates (error bars are mean ± SD) (A) D-IRK activity toward various synthetic peptide substrates was measured to determine the best peptide substrate. (B) Phosphorylation of E4YM4 peptide by D-IRK was carried out in buffer containing 4.67 mM each of $MgCl_2$, $MnCl_2$, or both.

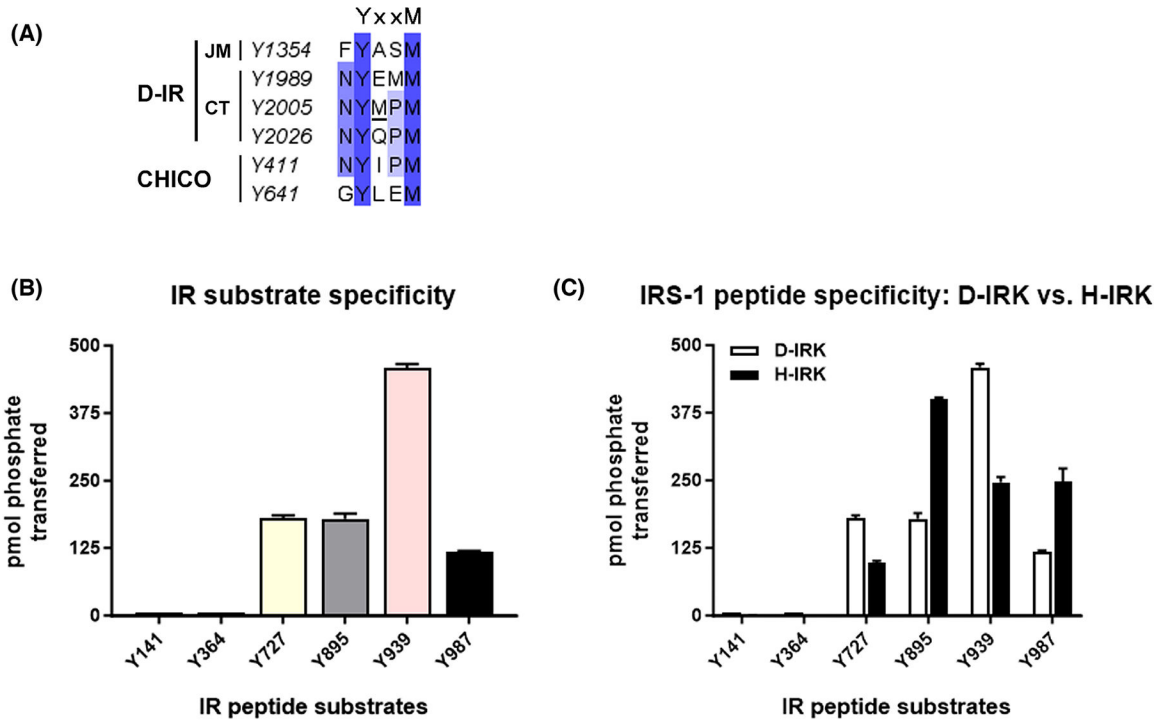

FIGURE 4.

Specificity of D-IRK for various IR substrate peptides. (A) YxxM motifs in the juxta-membrane and C-terminus of D-IR, and the *Drosophila* homolog of IRS-1 (CHICO) with the corresponding tyrosines numbered (according to NP_524436.2 for D-IR and NP_723540.1 for CHICO). Y2005 in the C-terminal of D-IR has a YMxM motif indicated by M. (B and C) Phosphorylation of synthetic peptides (0.5 mM) (sequences shown in Table 2) corresponding to rat β-adrenergic receptor (Y141 and Y364) and rat IRS-1 (Y727, Y895, Y939, and Y987) phosphorylation sites by Ni-NTA purified D-IRK (0.5 μM) (shown in (B) and (C)) or H-IRK (0.5 μM) (shown in (C)) were measured using the phosphocellulose paper-binding assays with [$\gamma-^{32}$ P]-ATP. Kinase activity is indicated as pmol of phosphate transferred onto the peptide substrates. Figures are a representative of two independent experiments each performed in duplicates (error bars are mean ± SD).

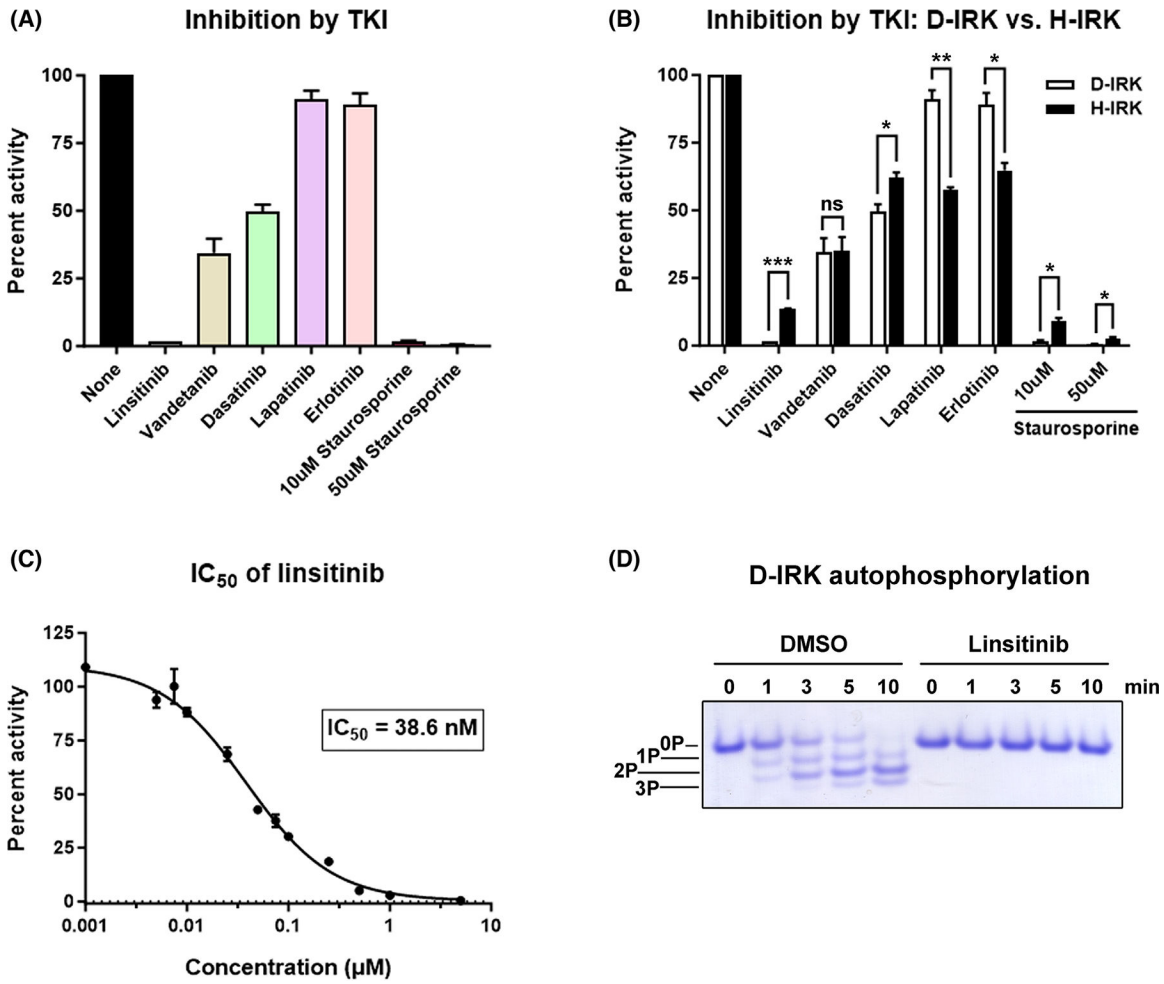

FIGURE 5.

Linsitinib inhibits D-IRK activity by blocking autophosphorylation. (A–C) Phosphorylation of E4YM4 peptide (0.5 mM) by Ni-NTA purified D-IRK (0.1 μM) or H-IRK (0.1 μM) (shown in (B)) in the presence of DMSO control (none) or indicated tyrosine kinase inhibitors (TKI) was measured using the phosphocellulose paper-binding assays with [$\gamma-^{32}$P]-ATP. Kinase activity is indicated as percent relative to DMSO control. Figures are a representative of two independent experiments each performed in duplicates (error bars are mean ± SD). (A) Activity of D-IRK was measured in the presence of various TKI at 10 μM concentrations (and 50 μM for staurosporine). (B) Activity of D-IRK in the presence of various TKIs as in (A) compared to that of H-IRK (0.1 μM). Multiple unpaired t-test was done to compute P values from the differences between D-IRK and H-IRK means. ***$p \leq .001$, **$p \leq .01$, *$p \leq .05$, $^{ns}p > .05$. (C) Half-maximal inhibitory concentration (IC_{50}) of linsitinib against D-IRK was determined to be 38.6 nM using a range of linsitinib concentrations as indicated. Figure shows non-linear fit (HillSlope = −1.028) of percent activities plotted against linsitinib concentrations (μM) displayed in a $\log_{10}$ scale. (D) D-IRK (2 μM) with or without linsitinib (10 μM) was autophosphorylated for the indicated time points and the three different autophosphorylated forms were analyzed by native PAGE followed by Coomassie staining.

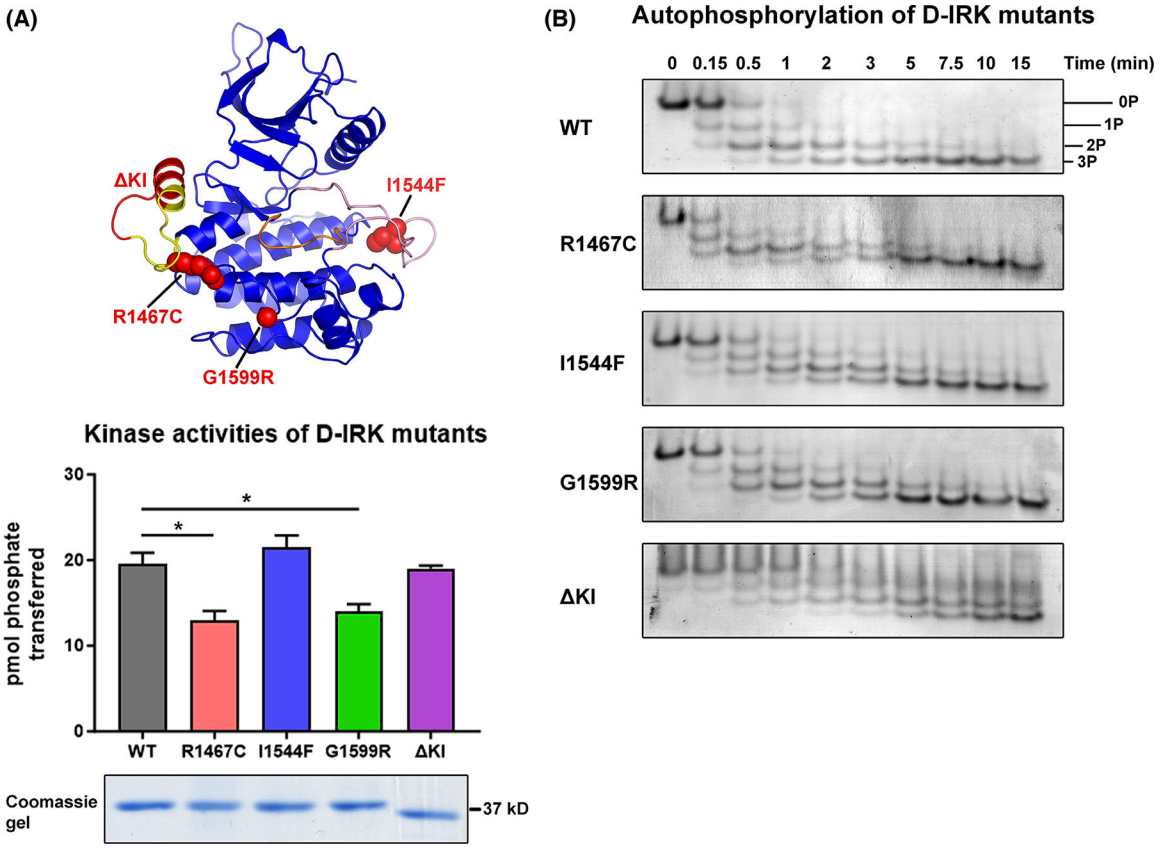

FIGURE 6.

Mutations in D-IRK have varying effects on catalytic activity. (A) *Top* AlphaFold predicted active structure of D-IRK (as in Figure 1B) with the point mutations (red spheres) and deletion (red ribbon) indicated (also described in Table 3). *Bottom* Kinase activity of WT or mutant D-IRK (0.1 μM) was measured using the phosphocellulose paper-binding assay with [γ–^{32}P]-ATP and is indicated as pmol of phosphate transferred on E4YM4 peptide (0.5 mM) in 5 min at 30°C. The figure is a representative of two independent experiments each performed in duplicates (error bars are mean ± SD, $*p \leq .05$ is derived from unpaired t-test). Below this is the Coomassie-stained PAGE gel of 0.2 μg of Ni-NTA purified WT and mutant D-IRKs. (B) Unphosphorylated (0P) and the three autophosphorylated forms (1P, 2P, and 3P) of WT and mutant D-IRKs were detected on native PAGE visualized by Coomassie staining. Autophosphorylation reactions were carried out using 2–3 μg of protein, 2 mM ATP, and 2 mM $MgCl_2$ at room temperature for the indicated time points.

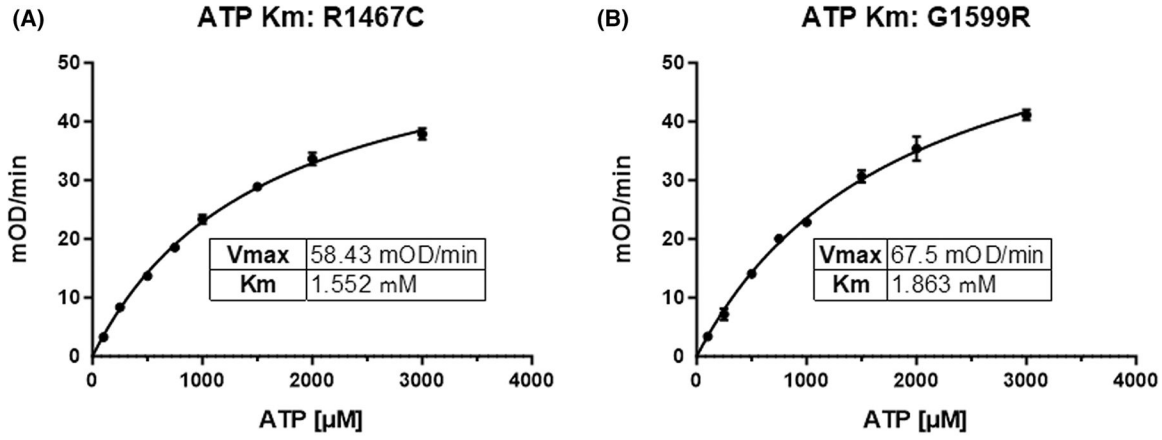

FIGURE 7.

D-IRK R1467C and G1599R mutants display altered kinetic parameters. Continuous spectrophotometric assays were performed in duplicate to determine the V_{max} and K_m of ATP of R1467C (A) and G1599R (B) mutations of D-IRK using 0.5 μM enzyme, 2 mM E4YM4 peptide substrate, and 100–3000 μM ATP. Figure shows slopes of NADH oxidation (mOD/min) plotted against the ATP concentrations fit to the Michaelis–Menten equation and the kinetic constants obtained.

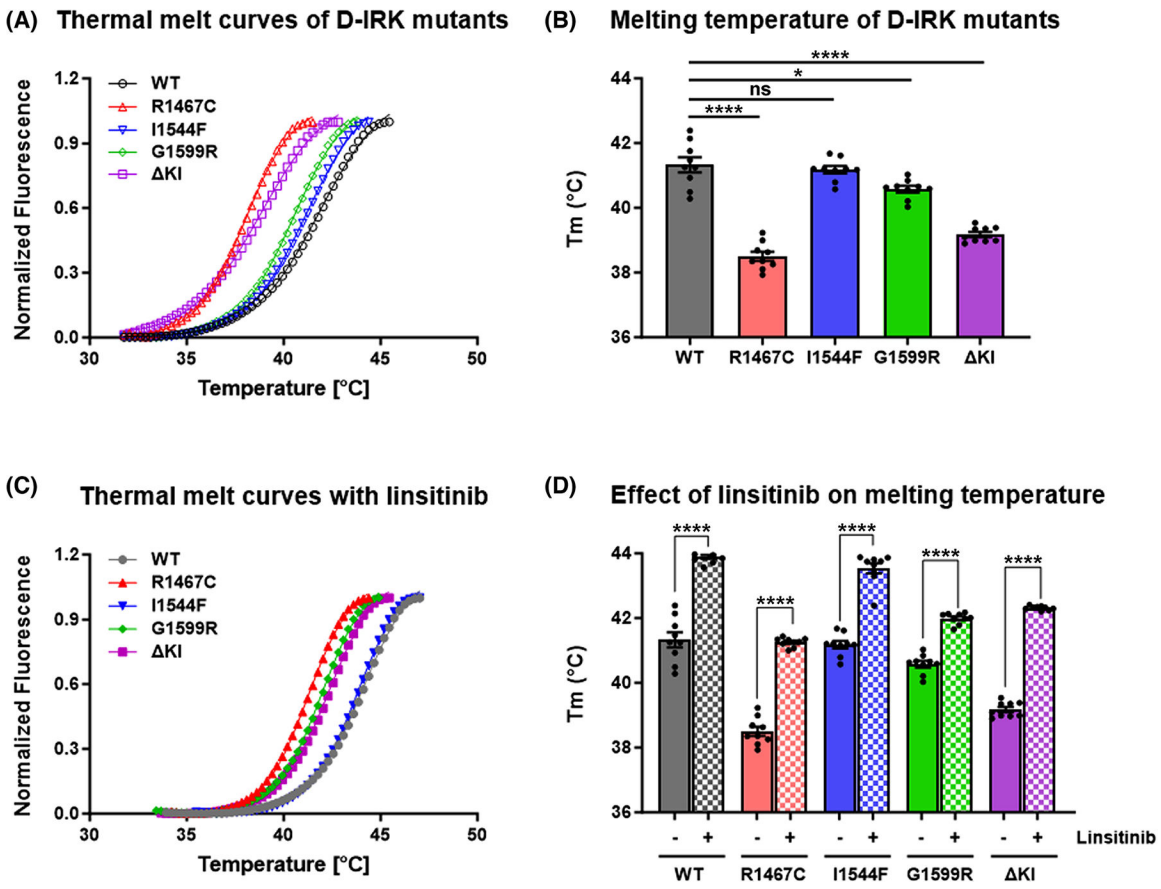

FIGURE 8.

D-IRK mutations have varying impacts on thermal stability but do not affect linsitinib binding. Thermal melt curves of WT and mutant D-IRKs (2 μM) were derived using fluorescence-based thermal shift assays. A representative of three independent experiments each done in triplicate with DMSO (A) or linsitinib (10 μM) (C) is shown. Melting temperatures (T_m) of WT and mutant D-IRKs with DMSO (B) or linsitinib (D) were determined from normalized melt curves fit to the Boltzmann equation. Figures show data from three independent experiments each done in triplicate (error bars are mean ± SEM, $n = 9$). One-way ANOVA was performed to compute p values. ****$p \leq .0001$, *$p \leq .05$, $^{ns}p > .05$.

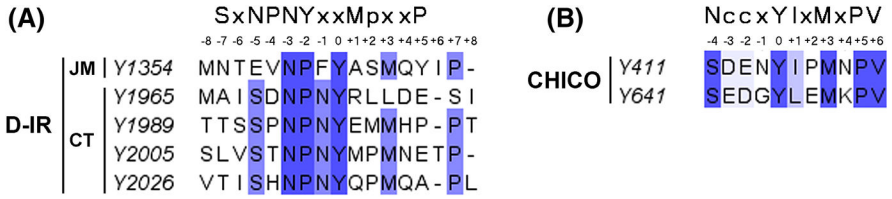

FIGURE 9.

Conserved motifs within D-IR and CHICO. Tyrosines (numbered according to NP_524436.2 for D-IR and NP_723540.1 for CHICO) present in YxxM motifs along with flanking sequences present in D-IR or CHICO were aligned using CLUSTALW. Aligned sequences were visualized and color-coded in Jalview, and manually annotated. The darker columns represent the alignment of identical amino acid residues, whereas the lighter colors represent the alignment of less conserved residues. *Lowercase letters* indicate conserved classes of amino acids as follows: x, any residue; p, polar residues; c, charged residues; l, aliphatic residues. (A) All of the tyrosines in YxxM motifs and one tyrosine in a YxxL motif located in the D-IR juxta-membrane and C-terminus regions are also part of a highly conserved NPxY motif. The C-terminus of D-IR has a conserved serine at the −5 and asparagine at the −1 positions relative to the target tyrosine which are absent in the juxta-membrane region. (B) CHICO YxxM motif contains two acidic residues in the −2 and −3 positions.

TABLE 1

Peptide substrate sequences of various kinases.

Kinase	Peptide substrate sequence
IR/IGF-1R	KKEEEEE**Y**MMMMG
PKA	LRRA**S**LG
Src	AEEEI**Y**GEFEAKKKKG
EGFR	AEEEE**Y**FELVAKKKG
Abl	EAI**Y**AAPFAKKKG
Ack1	KVI**Y**DFIEKKG

TABLE 2

Peptide sequences corresponding to IR substrates.

Peptide substrate type	Peptide name	Peptide sequence
Rat β-adrenergic receptor	Y141	KKSPFK**Y**QSLLTG
	Y364	KKGKTD**Y**MGEASG
Rat IRS-1	Y727	KKKLATGD**Y**MNMSPVG
	Y895	KKKSPGE**Y**VNIEFG
	Y939	KKREETGSEE**Y**MNMDLG
	Y987	KKSRGD**Y**MTMQIG

TABLE 3

D-IRK mutations.

Mutation	Location	Corresponding *Drosophila* allele
R1467C	Kinase insert domain	*InR*^{353}
I1544F	Activation loop	*InR*^{74}
G1599R	C-terminal lobe	*InR*^{211}
ΔKI	Deletion of ^{1476}MTYLNRIGVTGN^{1487} residues in the kinase insert domain	None

FASEB J. Author manuscript; available in PMC 2024 July 29.